RSC Advances

RSC Publishing

PAPER

View Article Online
View Journal | View Issue

Cite this: *RSC Advances*, 2013, **3**, 6369

A novel biomass coated Ag–TiO_2 composite as a photoanode for enhanced photocurrent in dye-sensitized solar cells

Zhongbiao Tian, Liqing Wang, Lishan Jia,* Qingbiao Li, Qianqian Song, Shuai Su and Hui Yang

Received 14th January 2013,
Accepted 21st February 2013

DOI: 10.1039/c3ra40195b

www.rsc.org/advances

A novel biomass-coated Ag nanoparticle-modified TiO_2 composite was prepared and used as a photoanode in a dye-sensitized solar cell with a high surface area, strong light scattering and efficient electron transport. It was found that syzygium extract has an appreciable effective function as a reducing and stabilizing agent simultaneously. The mean size of the synthesized silver nanoparticles is 4.0 $\pm$ 0.7 nm measured on the TEM images. Residual hydroxyl groups of the biomass on the photoanode improve dye absorption and electron injection efficiency. The syzygium-Ag–TiO_2 DSSC exhibits the best performance with a short-circuit current of 11.8 mA cm^{-2} corresponding to a photoelectric conversion efficiency of 5.12%, which is higher than the glucose-Ag–TiO_2 and UV-Ag–TiO_2 DSSCs, and much higher than the blank DSSC.

Introduction

For decades, titanium dioxide (TiO_2) nanoparticles have been the backbone of photoanode materials for developing high performance DSSCs because of their high specific surface area, which essentially occupies a large amount of dye molecules. However, electron transport in disordered TiO_2 nanoparticles proceeds by a trap-limited diffusion process, in which injected electrons travel through a large number of colloidal nanoparticles and grain boundaries before reaching the destination electrode. Such random photoelectron movement increases the chances of carrier recombination and thus decreases the efficiency of DSSCs.[1–4] This deficiency can be improved by a localized surface plasmon method. Although the claim was not thoroughly investigated, the concept of using plasmon-enhanced dye adsorption in DSSCs has been introduced in the literature.[5–7] The localized surface plasmon resonance effects enhance optical phenomena such as Raman scattering and light absorption.[8,9] A tested convenient way to build a LSPR-active substrate is to use silver (Ag) or gold (Au) nanoparticles, wherein Ag is generally preferred over Au having better LSPR active elements.[10] Moreover, silver nanoparticle doped TiO_2 nanoparticles also improve the electron transport in photoanodes, thereby enhancing the electron supply efficiencies of DSSCs.[11,12] Notably, Ihara *et al.*[13] found that when polymer-modified Ag nanoparticles were inserted in the pores of a TiO_2 film in DSSCs, photoelectric conversion efficiency therein was improved significantly by localized surface plasmon effects. Also Lin *et al.*[14] investigated FTO/TiO_2/NPs–Ag and FTO/NPs–Ag/TiO_2 cells, and compared to the standard electrode the results indicated that only the FTO/TiO_2/NPs–Ag electrode with substantial plasmon structure resulted in an enhanced photocurrent response. The observed effect was derived from an enhancement in the charge-separation efficiency induced from plasmon light scattering. Similarly, Han *et al.*[11] used photo-deposited Ag nanoparticles on a thin TiO_2 film anode in DSSCs and found that the electron transmission efficiency of the anode was elevated.

A number of approaches are available for the synthesis of silver nanoparticles *viz.* a photochemical method,[15] thermal decomposition of silver compounds,[16] an electrochemical method,[17] and recently *via* a green chemistry route.[18,19] Apparently, many of the nanoparticle synthesis methods are expensive and selectively involve the use of hazardous chemicals. The hazardous chemicals can cause contamination on the surface of the nanoparticle similar to the adverse effects of metals in applications. Above all, the biosynthesis of nanoparticles is highly favoured on account of its environmental friendliness, and is a method which has attracted considerable attention for materials' synthesis.[20] Plant leaves or plant seed extracts contain reducing sugars (aldoses), terpenoids, amino acids, and other organic compounds,[21] which are vital to cause changes in nanoparticle formation. Some of the extracts are composed of reducing agents, complexing agents and stabilizers which have an effect on the size and shape of the forming nanoparticles. In our previous work, we demonstrated that noble metal nanoparti-

Department of Chemical and Biochemical Engineering, College of Chemistry and Chemical Engineering, Xiamen University, Xiamen 361005, Fujian, China. E-mail: jials@xmu.edu.cn

cles reduced by biomass had excellent performance for photochemical catalysis and selective hydrogenation.[22,23]

In the present investigation, Ag nanoparticle doped TiO_2 nanoparticles were fabricated by silver reduction and used for the photoanode. The silver nanoparticles were reduced in the aqueous leaf extract of *Syzygium samarangense* without the use of toxic chemicals as reducing and stabilizing agents. The results showed that the addition of silver enhanced the optical absorption of the dye by localized surface plasmon resonance and improved the electron transfer through the formation of a conductive percolation network. Moreover, residual hydroxyl groups of the syzygium extract coated on the photoanode also improve the dye absorption and electron injection efficiency. These findings tremendously contributed to an increased photocurrent and corresponding improved efficiency in the DSSCs.

Experimental

Material

The fresh *Syzygium samarangense* leaves harvested from Fujian Province, China were spread in an oven at a controlled drying temperature. Optically transparent FTO conducting glass (fluorine doped SnO_2, transmission >90% in the visible region, sheet resistance 15 Ω/square) and electrolyte [containing 0.05 M iodine (I_2), 0.5 M lithium iodide (LiI), 0.3 M 1,2-methyl-3-propylimidazolium iodide, and 0.5 M 4-*tert*-butylpyridine in 3-methoxypropionitrile] were obtained from the Geao Science and Education Co. Ltd. of China. N719 dye [*cis*-bis(isothiocyanato)bis(2,2′-bipyridyl-4-4′dicarboxylato)–ruthenium(II)bis-tetrabutylammonium] was obtained from Solaronix.

Extract mixture

A measure of 3 g of ground *Syzygium samarangense* leaves was mixed with 80 ml deionized water and continuously boiled for 10 min. The filtrate of the cooled mixture was diluted to 100 ml in a volumetric flask. Furthermore, an accurately measured amount of 4 mg ml^{-1} of this solution was effectively used for silver (Ag^+ ions) reduction.

The silver doped TiO_2 nanoparticles

A suspension of TiO_2 (2 g, Degussa P25), 2 M $AgNO_3$ (125 μl), and proportionally 50 v% ethanol (50 ml), was constantly stirred in a water bath at 60 °C for 4 h. The previously prepared syzygium extract solution (50 ml) was added to the suspension and further constantly stirred at 90 °C for 90 min. Next, the mixture was filtered and thoroughly washed with deionized water to remove the excess syzygium extract. The dark brown product in powder form was dried at 80 °C for 24 h. The material synthesised with 1.3 wt% Ag doped TiO_2 is hereafter named syzygium-1.3%Ag–TiO_2.

Silver doped TiO_2 nanoparticles reduced by a chemical method (glucose-1.3%Ag–TiO_2) and a photochemical method (UV-1.3%Ag–TiO_2) were also prepared. The primary constituent materials used in the chemically reduced method include glucose and a protecting agent, polyvinylpyrrolidone (PVP). In a similar suspension medium as above, a mixture of glucose (3 g), PVP (1 g) and deionized water (50 ml) was adjusted to pH = 11 with 1 M NaOH and stirred in a water bath maintained at 70 °C. The resultant TiO_2 and $AgNO_3$ suspension was added to the glucose solution drop-wise over a 2 h reaction period. 2 g of TiO_2 powder in an aqueous solution of $AgNO_3$ (2 M, 125 μl) was completely mixed with 100 mL of H_2O to form the 1.3 wt% Ag photo-deposited on TiO_2. The suspension was illuminated by a Hg lamp (125 W) for 30 min and the precipitate which formed was filtered, washed with deionized water and dried at 80 °C for 24 h.

DSSC assembly

The two DSSCs assembled for comparison were comprised of pure TiO_2 nanoparticle films and silver doped TiO_2 nanoparticle films. Prior to assembly, a pre-assembly of the DSSC parts were prepared as follows; in a conventional synthesis of a photoanode,[24,25] samples of FTO-coated glass with dimensions 15 × 20 mm^2 were refluxed in 40 mM $TiCl_4$ aqueous solution at 70 °C for 30 min and calcined at 450 °C for 30 min to form the first layer. TiO_2 nanoparticles were mixed with PEG-20000 in water containing some acetyl acetone and Triton X-100 to form a paste, and the paste was deposited on the FTO sample by dip-coating to obtain a transparent TiO_2 layer which was heated at 450 °C for 30 min. Again, the sample was immersed in 40 mM $TiCl_4$ aqueous solution and annealed, cooled to 80 °C and immersed in 0.5 mM solution of N719 dye in ethanol for 24 h. These pre-assembled parts were integrated into a solar cell with Pt-coated FTO glass counter electrodes, wherein each cathode–anode pair was combined with a 60 μm thick Surlyn polymer film. Further, the electrolyte was injected into the internal space of the cell. Evaluation of the photovoltaic performance was carried out systematically.

Characterization

A standard Philip Analytical FEI Tecnai 30 electron microscope was used at an accelerating voltage of 300 kV for high resolution transmission electron microscopy (HRTEM) characterization of the metallic particle morphology. The size distribution of the particles was estimated from TEM images using Sigma Scan Pro software (SPSS Inc., version 4.01.003). An FTIR Nicolet Avatar 360 (Nicolet, USA) was used for spectral analysis and spectra were recorded in the region 4000–400 cm^{-1} at a resolution of 4 cm^{-1} with 32 applied scans. X-ray photoelectron spectroscopy (XPS) analyses were performed on a PHI Quantum 2000 Scanning ESCA microprobe with a monochromatized micro-focused Al X-ray source. The binding energy was calibrated using C1s as the reference energy (C1s = 284.8 eV). Visible region extinction spectra of dyes and electrodes were recorded on a Varian Cary 5000 UV-vis-NIR spectrophotometer. Photocurrent density–applied voltage (*I–V*) and electrochemical impedance spectroscopy (EIS) measurements of the DSSCs were obtained using a home-built setup comprising a xenon lamp, an AM 1.5 light filter, and a CHI660D Electrochemical Analyzer (CHI instruments). The power of the filtered light was calibrated by a China National Institute of Metrology certified silicon reference cell to 100 mW cm^{-2}.

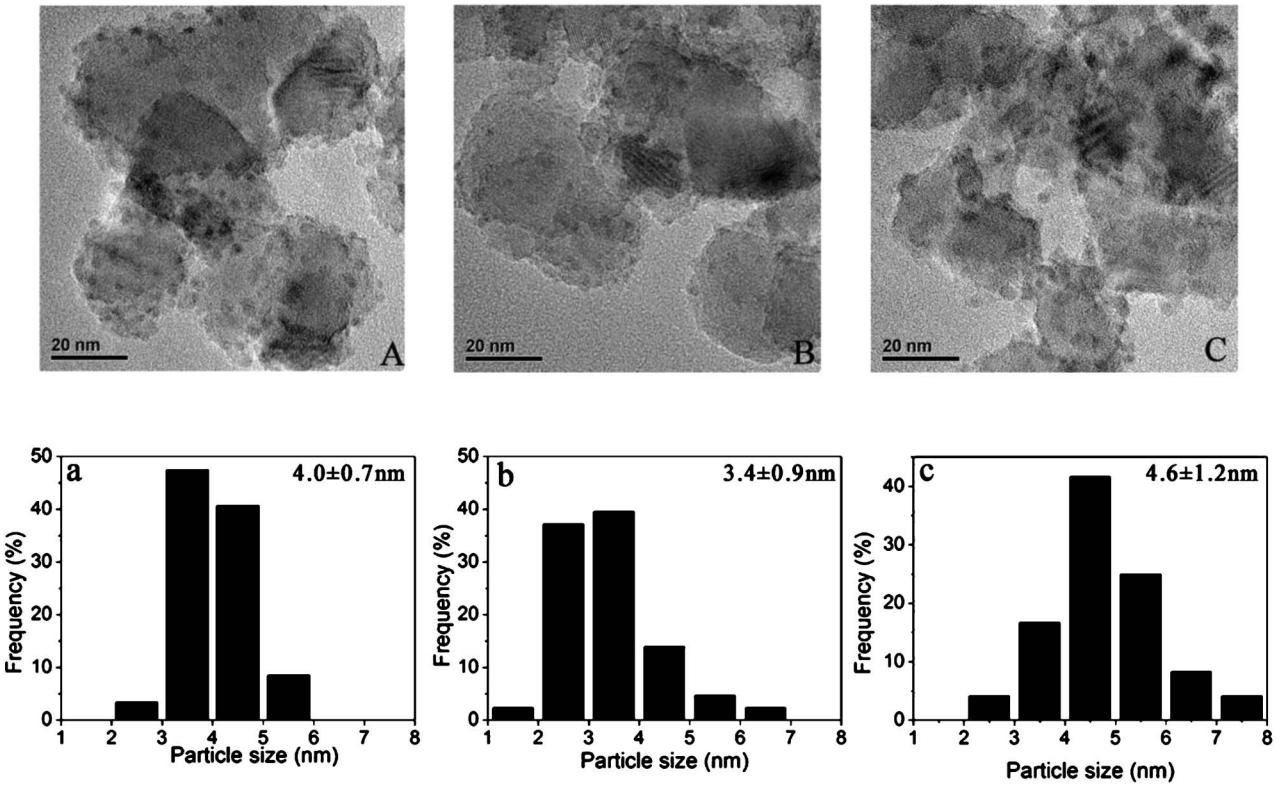

Fig. 1 TEM and silver nanoparticles size distributions of the syzygium-1.3%Ag–TiO_2 photoanode (A, a), the glucose-1.3%Ag–TiO_2 photoanode (B, b) and the UV-1.3%Ag–TiO_2 photoanode (C, c).

Results and discussion

Fig. 1 shows the photoanode TEM images and particle size distributions of Ag doped TiO_2 nanoparticles reduced by syzygium extract, glucose, and UV light. Due to the contrastive distinction, Ag deposited on TiO_2 could be readily identified as black spots superimposed on the background of the larger TiO_2 particles. The mean particle sizes estimated on the basis of TEM images from A, B, and C were found to be 4.0 $\pm$ 0.7 nm, 3.4 $\pm$ 0.9 nm, and 4.6 $\pm$ 1.2 nm respectively. As can be observed in Fig. 1(A), the Ag nanoparticles reduced by syzygium with sizes of about 4 nm in diameter are evenly dispersed on the larger TiO_2 grains and TiO_2 agglomerates. The same almost spherical shape, similar size and good distribution could be attributed to the stabilizing function of the syzygium extract as aforementioned.[26,27] In comparison with Fig. 1(A), the silver nanoparticles reduced by the glucose solution [Fig. 1(B)] are distributed evenly on the TiO_2 substrate and their average diameter is smaller than the silver nanoparticles reduced by syzygium extract. In Fig. 1(C) the silver nanoparticles reduced by UV light are sparsely dispersed on the TiO_2 substrate and have a widespread particle size distribution and aggregation. Previous studies have shown that DSSCs made from Ag nanoparticles with sizes less than 4.5 nm demonstrated a better photoelectric conversion efficiency, and the best absorption enhancement was obtained with a Ag film thickness of 3 nm.[28,29]

FT-IR measurement was carried out to investigate the preparation process of syzygium-Ag–TiO_2 nanoparticles. The bands are identified in Fig. 2 along the trend profiles labelled a–d. Trend (a) is the spectrum of TiO_2 (Degussa P25), and the broad band at 3427 cm^{-1} is assigned to O–H representing the stretching vibration of Ti–OH. The band at 1640 cm^{-1} is assigned to the O–H bending mode of the hydroxyl groups or to the stretching mode of Ti–O,[30] and the band at 1124 cm^{-1} is

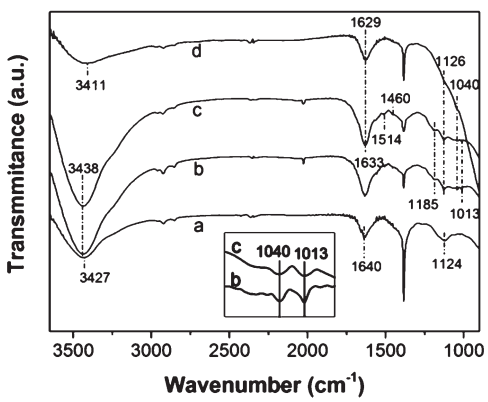

Fig. 2 Fourier transform infrared spectra of Degussa P25 nanoparticles (a), syzygium-TiO_2 nanoparticles (b), syzygium-1.3%Ag–TiO_2 nanoparticles (c), and syzygium-1.3%Ag–TiO_2 nanoparticles annealed at 450 °C for 30 min (d).

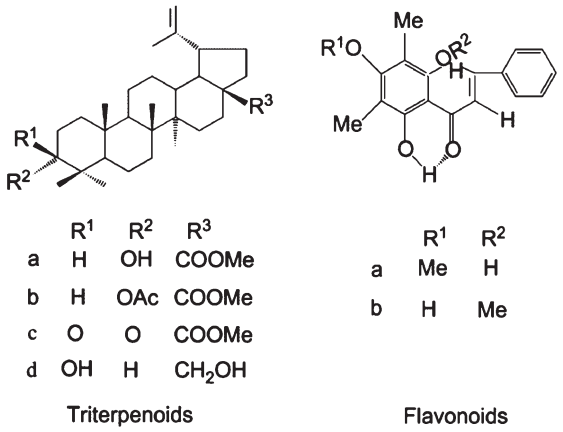

Fig. 3 Structures of some triterpenoids and flavonoids.

assigned to the graphitic carbon of combustion in synthesized TiO_2.[31] The peaks on trend (d) deviated from (a) to 3411 and 1629 cm^{-1} and the peak at 3411 cm^{-1} becomes slightly smaller after doping with Ag nanoparticles. These suggest that the Ag nanoparticles interact with TiO_2. For trend (b), P25 was treated with syzygium extract and the band ranges at 1185, 1040, and 1013 cm^{-1} were assigned to C–O representing the vibrations of carboxylic acids, alcohols and phenol.[32,33] Triterpenoids and flavonoids are the main components of the crude water extract, which are both antioxidants.[34,35] Fig. 3 shows their structures. Carbonyl, carboxyl, and especially abundant hydroxyl groups were determined in their structures. The evolution of the peaks indicates that syzygium extract biomass coats the TiO_2 surface. The peaks at 1040 and 1013 cm^{-1} tend to be flat, as shown in trend (c), after the addition of aqueous silver nitrate ($AgNO_3$) solution and this could be attributed to the reduction of Ag^+ by C–O–H. The peaks at 1514 and 1460 cm^{-1} emerge after Ag^+ is reduced to metallic Ag, which implies that the surface coating by C=C and C=O bonds[21] contributes to the reduction and stabilization of silver nanoparticles, and may influence the crystal growth of the silver nanoparticles. All these phenomena prove that syzygium extract functions as both a reducing and stabilizing agent and deposits on the surface of Ag–TiO_2. After heat treatment at 450 °C for 30 min during the preparation of the photoanode [see trend (d)], the peak at 1040 cm^{-1} still exists which could be due to the presence of C–O–H on the Ag and TiO_2 nanoparticles, which may improve the dye absorption in the photoanode.

Fig. 4 and Fig. 5 show the XPS spectra of the syzygium-1.3%Ag–TiO_2 (a), glucose-1.3%Ag–TiO_2 (b), and UV-1.3%Ag–TiO_2 (c) photoanodes. Particular attention was given to the binding energies of the O 1s and Ag 3d components. As shown in Fig. 4, two ranges of oxygen peaks at 529.7–530.2 eV and 530.7–530.8 eV appeared in spectra (a), (b), (c), and (d). The first range is attributed to Ti–O in the bulk form, and the second is attributed to Ti–O on the surface.[11] Syzygium-1.3%Ag–TiO_2 produced a peak at 532.4 eV, which is attributed to oxygen in phenolic hydroxyl (C–OH) groups.[36,37] In Fig. 4(b), the peak at 530.2 eV is slightly shifted to a higher binding

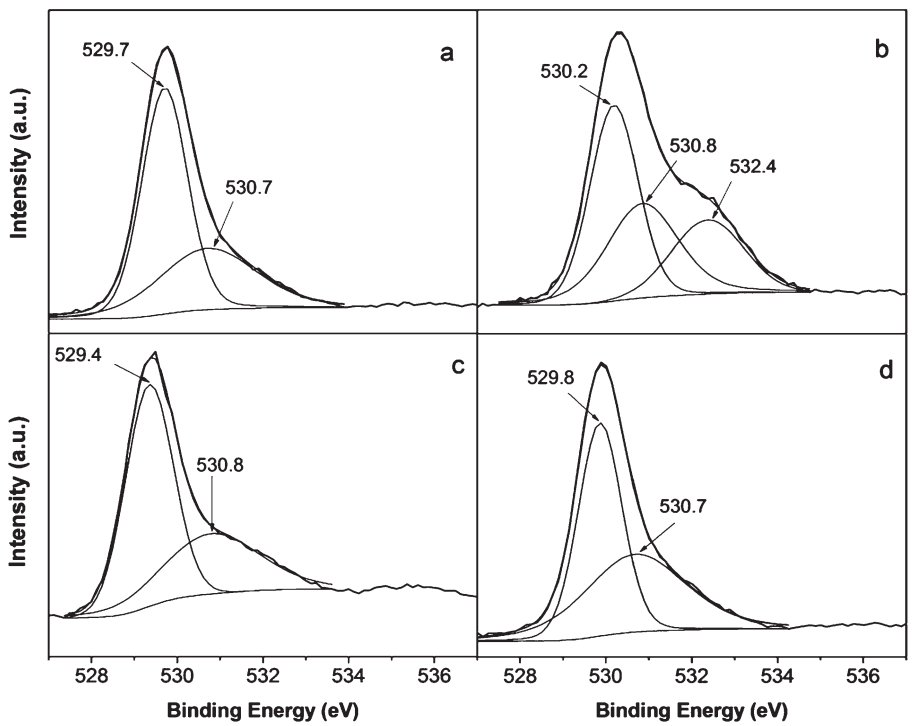

Fig. 4 X-ray photoelectron spectra of Degussa P25 (a), syzygium-1.3%Ag–TiO_2 (b), glucose-1.3%Ag–TiO_2 (c) and UV-1.3%Ag–TiO_2 (d) photoanodes, showing the O 1s region with the fitting result.

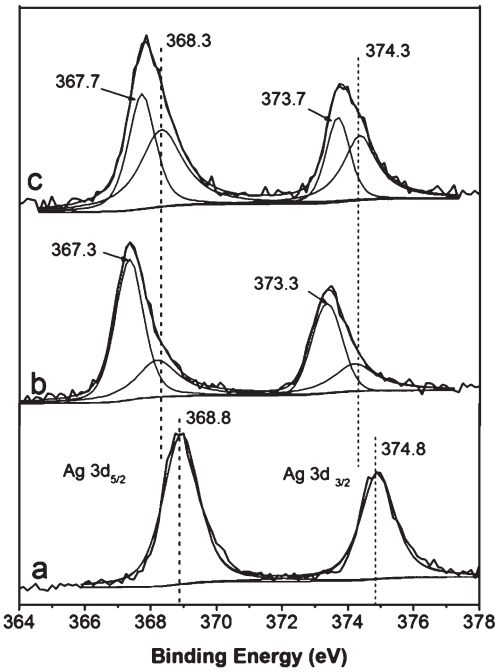

Fig. 5 The Ag 3d region of the XPS spectra of the syzygium-1.3%Ag–TiO_2 (a), glucose-1.3%Ag–TiO_2 (b), and UV-1.3%Ag–TiO_2 (c) photoanodes.

energy relative to Fig. 4(a), (c) and (d), which indicates a partial increase in the electron density around the O atoms due to the interaction of residual organic groups with TiO_2. Fig. 5 shows the narrow scans for the Ag 3d region. In Fig. 5(b) and (c), Ag ($3d_{5/2}$ and $3d_{3/2}$) peaks are observed at binding energies of 368.3 and 374.3 eV with a peak separation of 6 eV. These values correspond well to metallic silver.[38] The binding energies at 367.3, 367.7, 373.3 and 373.7 eV correspond to oxidized silver.[32] This indicates that Ag exists as a mixture of metallic and oxidized silver in the glucose-1.3%Ag–TiO_2 and UV-1.3%Ag–TiO_2 photoanodes. However, in Fig. 5(a), Ag ($3d_{5/2}$ and $3d_{3/2}$) peaks are observed at binding energies of 368.8 and 374.8 eV, where a shift of 0.5 eV emerges compared to Fig. 5(b) and 5(c). The Ag in the syzygium-1.3%Ag–TiO_2 sample is still neutral silver.[39,40] The positive shift of the binding energy may be due to the particle size or chemical and charge effects.[41,42] As shown in Fig. 1, the size of silver nanoparticles reduced by syzygium extract is located between that of the silver nanoparticles reduced by glucose solution and UV light. Therefore, the shift of peak values to a higher binding energy should be due to chemical and charge effects. This change is also attributable to the interaction of residual organic groups with the Ag–TiO_2 nanoparticles, which provide electropositive surroundings[43] and capture photoinduced cavities to improve electron transfer in the photoanode.

The absorption spectra of the photo-absorbing layers of the DSSCs with and without silver nanoparticles are depicted in Fig. 6. Remarkably, the spectra of the materials containing Ag nanoparticles are elevated above the ones without Ag nanoparticles. Generally, absorption increased as the amount

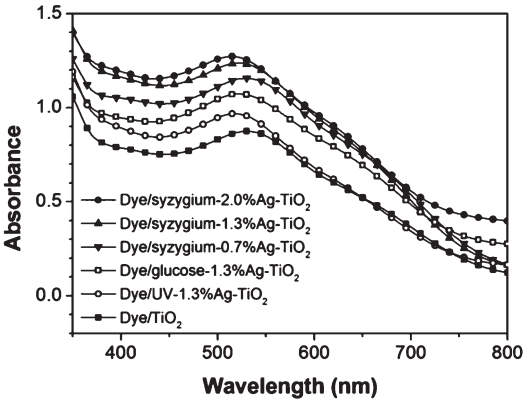

Fig. 6 Absorption spectrum of the photo-absorbing layers of DSSCs.

of Ag increased (syzygium-0.7%Ag–TiO_2, syzygium-1.3%Ag–TiO_2, syzygium-2.0%Ag–TiO_2).[14] The strong optical absorption in the doped DSSC sample is due to the influence of the plasmon effect caused by the presence of Ag nanoparticles. The light illumination of Ag nanoparticles on dielectric surfaces apparently absorbs the resonating light wavelength agitated by the electron plasma frequency and hence creates a greatly enhanced electromagnetic field near the Ag nanoparticle surface.[12] However, the magnitude of the plasmon effect is obviously relative to the interactions between the Ag nanoparticles and the dye, so the light-matter interaction is stronger for smaller relative distances.[44] Therefore, the localized electromagnetic field around the Ag nanoparticles strongly enhances the optical absorption efficiency of the dye molecules. Proportionately, the photocurrent of the Ag nanoparticle doped DSSC sample increased. At this juncture, the syzygium-1.3%Ag–TiO_2 film integrated with a dye coating records the highest optical absorption (syzygium-1.3%Ag–TiO_2, glucose-1.3%Ag–TiO_2 and UV-1.3%Ag–TiO_2). The Ag doped TiO_2 nanoparticles formed using the syzygium extract reduction demonstrated a better resonant ability.

Fig. 7 shows the measured *I–V* characteristics of the blank DSSC and silver doped DSSCs exposed to a 100 mW cm^{-2} light source from a solar simulator. The photoelectric energy conversion efficiency (η), open circuit voltage (V_{oc}), short circuit current (I_{sc}), and fill factor of the cells (*ff*) were determined from these measured *I–V* characteristics (see Table 1). Shown in Fig. 7(a) is the typical increase in I_{sc} because of the increased amount (from 0 to 1.3 wt%) of Ag, but, conversely, further increasing the loading amount of Ag decreases the I_{sc}. The V_{oc} of syzygium-Ag–TiO_2 DSSCs made in this research ranks above the blank DSSC counterpart. The efficiency of the blank DSSC was about 3.35%, whereas the efficiency of the syzygium-1.3%Ag–TiO_2 DSSC improved to 5.12%. Such an improvement was due to increasing the I_{sc}. In Fig. 7(b), the I_{sc} increased from 7.48 mA cm^{-2} (blank DSSC) to 8.36 mA cm^{-2} (UV-1.3%Ag–TiO_2 DSSC), 10.72 mA cm^{-2} (glucose-1.3%Ag–TiO_2 DSSC), and 11.80 mA cm^{-2} (syzygium-1.3%Ag–TiO_2 DSSC) respectively. All the Ag doped DSSCs

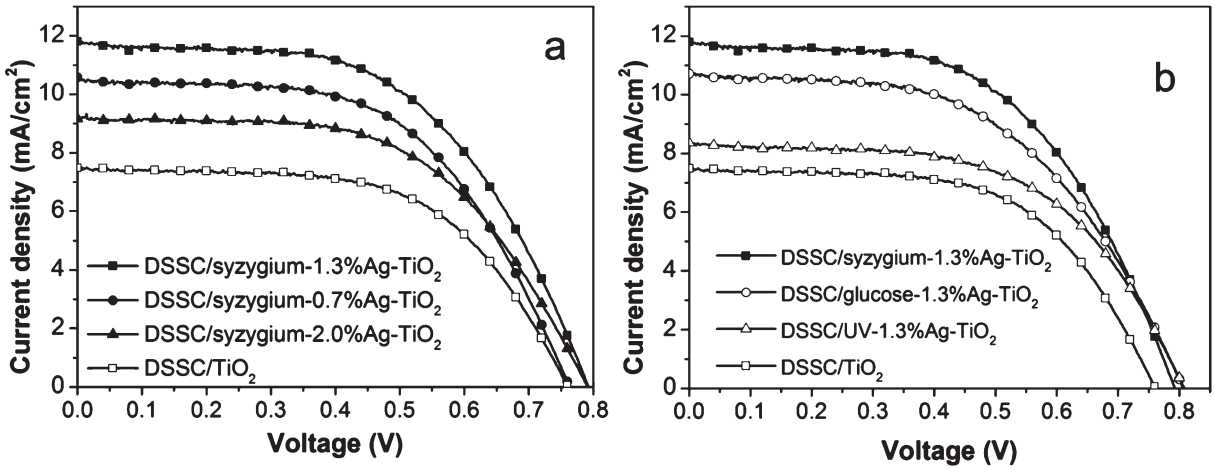

Fig. 7 Current density (*I*) *versus* voltage (*V*) curves under AM 1.5 conditions (100 mW cm^{-2}); (a) TiO_2, syzygium-0.7%Ag–TiO_2, syzygium-1.3%Ag–TiO_2 and syzygium-2.0%Ag–TiO_2 DSSCs; (b) TiO_2, UV-1.3%Ag–TiO_2, glucose-1.3%Ag–TiO_2 and syzygium-1.3%Ag–TiO_2 DSSCs.

exhibited better photoelectric performances, and the biomass coated Ag–TiO_2 DSSC was the best. Additionally, it was observed that the V_{oc} values of the Ag doped DSSCs were about 800 mV, higher than that of the blank DSSC which, as shown in Table 1, was 761 mV.

Based on these results, the interest in understanding the enhanced short circuit current density in the Ag doped DSSCs discussed in this study motivated the use of a dye desorption experiment which involved measuring the absorption spectrum of a mixed solution of 0.1 M NaOH and ethanol (1 : 1 v/v). The dye-loading of DSSCs with and without silver are shown in Table 1. The absorbance of N719 in syzygium-1.3%Ag–TiO_2, glucose-1.3%Ag–TiO_2 and UV-1.3%Ag–TiO_2 were 1.4, 1.2 and 1.2 times higher than that in TiO_2, respectively. An increase in the surface area of Ag doped TiO_2 nanoparticles could contribute to this increase.[45] Syzygium-1.3%Ag–TiO_2 absorbs more dye, which can be attributed to the residual organic groups of the syzygium extract in the photoanode. The short current densities in the syzygium-1.3%Ag–TiO_2, glucose-1.3%Ag–TiO_2 and UV-1.3%Ag–TiO_2 DSSCs were 1.6, 1.4 and 1.1 times higher than that in TiO_2 DSSCs, respectively. For UV-1.3%Ag–TiO_2 with 1.2 times the dye absorption and 1.1 times the short current density, the effective amount of dye to generate a photocurrent in the Ag doped DSSCs should be less than that in the blank DSSCs.[46] Conversely, the 1.6-fold short current density in syzygium-1.3%Ag–TiO_2 cannot be explained only by the increase in adsorbed dye. The improvement in I_{sc} for the syzygium-1.3%Ag–TiO_2 DSSC was at least partially caused by the localized surface plasmon resonance effects. These results indicate that Ag doped TiO_2 nanoparticles reduced by syzygium extract are better for dye absorption and plasmon resonant enhancement.

Li[12] *et al.* utilized an electrospinning method to prepare Ag doped TiO_2 nanofibers to be used as photoanodes to fabricate dye sensitized solar cells. It was found that the silver nanoparticle doped solar cell had a conversion efficiency of 4.13% (Table 1, entry 5). Ihara[13] *et al.* fabricated TiO_2 films by spin coating the slurry onto conductive glass substrates, which were immersed in a colloidal solution of polymer-modified Ag nanoparticles to obtain a Ag–TiO_2 photoanode for DSSCs. The best DSSC showed a conversion efficiency of 2.5% (Table 1, entry 6). Compared with other analogous synthetic approaches, the biomass coating method is still superior.

The Nyquist plots obtained from devices based on TiO_2 nanoparticulate photoanodes with and without Ag doping under one-sun illumination are shown in Fig. 8. The spectra

Table 1 Current (*I*)–Voltage (*V*) parameters (I_{sc} = short-circuit photocurrent, V_{oc} = open-circuit voltage, η = efficiency, *ff* = fill factor) of different samples sensitized with N719 dye and amount of dye adsorbed on TiO_2 films

Entry	DSSC	I_{sc} (mA cm^{-2})	V_{oc} (mV)	*ff* (%)	η (%)	Amount (mol cm^{-2})	Reference
1	TiO_2	7.48	761	58.9	3.35	8.69×10^{-8}	This work
2	UV-1.3%Ag–TiO_2	8.36	808	56.7	3.83	1.07×10^{-7}	
3	glucose-1.3%Ag–TiO_2	10.72	806	52.3	4.54	9.96×10^{-8}	
4	syzygium-1.3%Ag–TiO_2	11.80	792	54.8	5.12	1.21×10^{-7}	
5[a]	Ag–TiO_2	9.51	780	56.0	4.13		12
6[b]	Ag–TiO_2	4.4	810	69.0	2.5		13

[a] Compositions: photoanode (Ag–TiO_2 nanofibers prepared by an electrospinning method); dye (N719); electrolyte (Iodolyte AN-50, Solaronix); counter electrode (Pt). [b] Compositions: photoanode (Ag–TiO_2 films prepared by an immersion method); dye ($Ru(bipy)_2(SCN)_2$); electrolyte (a 3-methoxypropionitrile solution of 4-*tert*-butylpyridine, lithium iodide, iodine, and dimethylpropylimidazolium iodide); counter electrode (Pt).

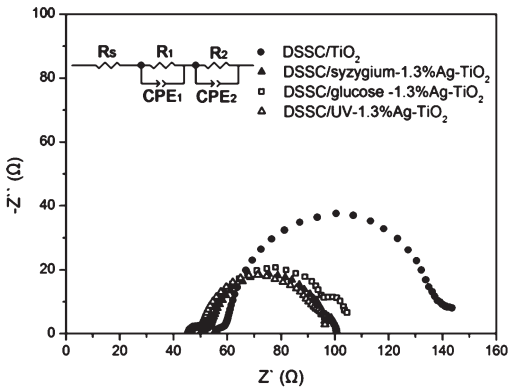

Fig. 8 Electrochemical impedance spectra of reference DSSC and DSSCs based on a silver doped TiO_2 electrode made by different reduction methods.

show three distinguishable semicircles, which are related to the electrochemical reactions at the Pt counter electrode (in the kHz range), at the metal oxide film–dye–electrode (in the range 1–1000 Hz) and the Warburg diffusion process of I^-/I_3^- (<1 Hz) from left to right, respectively.[47] The extent of electron transport in the photoanodes can be judged by the impedance, which is defined by the diameter of the middle semicircle.[48] Under one-sun illumination, the diameter of the silver doped TiO_2 nanoparticulate film is smaller than that of the non-doped TiO_2 nanoparticulate film, suggesting that there is less impedance at the silver doped photoanode surface which contributes to the charge transport in the photoanodes. The electrical behaviour of the cells under illumination was modelled by an equivalent electrical circuit as shown in Fig. 8. It was found that the charge transport resistances at the TiO_2–dye–electrolyte interface of TiO_2, UV-1.3%Ag–TiO_2, glucose-1.3%Ag–TiO_2, and syzygium-1.3%Ag–TiO_2 photoanodes estimated from Nyquist plots were 78.44 Ω, 41.9 Ω, 46.7 Ω and 36.0 Ω, respectively. It is reported that dyes with hydroxyls as anchoring groups in the syzygium-1.3%Ag–TiO_2 photoanode exhibited improved electron injection efficiency and overall photoelectric conversion efficiency.[49,50] In other words, the charge transfer resistance in syzygium-1.3%Ag–TiO_2 photoanodes is smallest, leading to an improvement in solar cell performance.

Conclusions

This study has systematically demonstrated a simple and effective method to prepare biomass coated Ag–TiO_2 photoanodes for dye sensitized solar cells. The syzygium extract acts as a reductant, complexing agent, and stabilizer, which in turn dictates the size and shape of the nanoparticles. The compared results reveal differences between the blank DSSC sample and the present study (syzygium-1.3%Ag–TiO_2 DSSC) with a 53% conversion efficiency improvement caused by a 57% short circuit current density enhancement. The dye absorption phenomenon is very effective due to residual hydroxyl group activity. Also, the optical absorption phenomenon was high because of the Ag plasmon effect and improved electron injection efficiency owing to the use of N719 dye with hydroxyl anchoring groups. The combination of these phenomena enhanced the performance of the DSSC system. The achieved objective of realizing light to electrical energy conversion in a dye sensitized solar cell was enabled by the use of specific materials. It is hoped that this work will provide a new impetus for low-cost technology for high light-to-electrical energy conversion in dye sensitized solar cells.

Acknowledgements

This research is supported by the Natural Science Foundation of Fujian Province of China (Grant No. 2010J01052), key program (Grant No. 21036004) of the National Natural Science Foundation of China and the general program of the National Natural Science Foundation of China (Grant No. 21176203).

References

1 B. O'Regan, L. Xiaoe and T. Ghaddar, *Energy Environ. Sci.*, 2012, **5**, 7203.
2 N. Kopidakis, N. Neale, K. Zhu, J. Van De Lagemaat and A. Frank, *Appl. Phys. Lett.*, 2005, **87**, 202106.
3 J. van de Lagemaat, K. D. Benkstein and A. J. Frank, *J. Phys. Chem. B*, 2001, **105**, 12433.
4 Y. B. Tang, C. S. Lee, J. Xu, Z. T. Liu, Z. H. Chen, Z. He, Y. L. Cao, G. Yuan, H. Song and L. Chen, *ACS Nano*, 2010, **4**, 3482.
5 S. D. Standridge, G. C. Schatz and J. T. Hupp, *J. Am. Chem. Soc.*, 2009, **131**, 8407.
6 W. Hou, P. Pavaskar, Z. Liu, J. Theiss, M. Aykol and S. B. Cronin, *Energy Environ. Sci.*, 2011, **4**, 4650.
7 J. Du, J. Qi, D. Wang and Z. Tang, *Energy Environ. Sci.*, 2012, **5**, 6914.
8 F. Liu, Z. Cao, C. Tang, L. Chen and Z. Wang, *ACS Nano*, 2010, **4**, 2643.
9 S. Chang, Q. Li, X. Xiao, Y. K. Wong and T. Chen, *Energy Environ. Sci.*, 2012, **5**, 9444.
10 M. Erol, Y. Han, S. K. Stanley, C. M. Stafford, H. Du and S. Sukhishvili, *J. Am. Chem. Soc.*, 2009, **131**, 7480.
11 Z. Han, Y. Yu, J. Zhang and W. Cao, *Mater. Lett.*, 2012, **70**, 193.
12 J. Li, X. Chen, N. Ai, J. Hao, Q. Chen, S. Strauf and Y. Shi, *Chem. Phys. Lett.*, 2011, **514**, 141.
13 M. Ihara, M. Kanno and S. Inoue, *Phys. E.*, 2010, **42**, 2867.
14 S. J. Lin, K. C. Lee, J. L. Wu and J. Y. Wu, *Sol. Energy*, 2012, **86**, 2600.
15 X. Lin, F. Rong, D. Fu and C. Yuan, *Powder Technol.*, 2012, **219**, 173.
16 S. Navaladian, B. Viswanathan, R. Viswanath and T. Varadarajan, *Nanoscale Res. Lett.*, 2006, **2**, 44.
17 L. Rodriguez-Sanchez, M. Blanco and M. Lopez-Quintela, *J. Phys. Chem. B*, 2000, **104**, 9683.
18 L. Lin, W. Wang, J. Huang, Q. Li, D. Sun, X. Yang, H. Wang, N. He and Y. Wang, *Chem. Eng. J.*, 2010, **162**, 852.

19 M. Du, G. Zhan, X. Yang, H. Wang, W. Lin, Y. Zhou, J. Zhu, L. Lin, J. Huang and D. Sun, *J. Catal.*, 2011, **283**, 192.
20 K. Mukunthan, E. Elumalai, T. N. Patel and V. R. Murty, *Asian Pac. J. Trop. Biomed.*, 2011, **1**, 270.
21 M. Yilmaz, H. Turkdemir, M. A. Kilic, E. Bayram, A. Cicek, A. Mete and B. Ulug, *Mater. Chem. Phys.*, 2011, **130**, 1195.
22 X. Wu, Q. Song, L. Jia, Q. Li, C. Yang and L. Lin, *Int. J. Hydrogen Energy*, 2012, **37**, 109.
23 L. Jia, Q. Zhang, Q. Li and H. Song, *Nanotechnology*, 2009, **20**, 385601.
24 M. Sun, W. Fu, H. Yang, Y. Sui, B. Zhao, G. Yin, Q. Li, H. Zhao and G. Zou, *Electrochem. Commun.*, 2011, **13**, 1324.
25 N. Fuke, R. Katoh, A. Islam, M. Kasuya, A. Furube, A. Fukui, Y. Chiba, R. Komiya, R. Yamanaka and L. Han, *Energy Environ. Sci.*, 2009, **2**, 1205.
26 D. MubarakAli, N. Thajuddin, K. Jeganathan and M. Gunasekaran, *Colloids Surf., B*, 2011, **85**, 360.
27 H. Bar, D. K. Bhui, G. P. Sahoo, P. Sarkar, S. Pyne, A. Misra and Surf. Colloids, *Colloids Surf., A*, 2009, **348**, 212.
28 C. Photiphitak, P. Rakkwamsuk, P. Muthitamongkol, C. Sae-Kung and C. Thanachayanont, *Int. J. Photoenergy*, 2011, DOI: 10.1155/2011/258635.
29 K. C. Lee, S. J. Lin, C. H. Lin, C. S. Tsai and Y. J. Lu, *Surf. Coat. Technol.*, 2008, **202**, 5339.
30 L. Gomathi Devi and K. Mohan Reddy, *Appl. Surf. Sci.*, 2011, **257**, 6821.
31 K. Nagaveni, G. Sivalingam, M. Hegde and G. Madras, *Appl. Catal., B*, 2004, **48**, 83.
32 A. Stuart and G. Sutherland, *J. Chem. Phys.*, 1956, **24**, 559.
33 A. Graveland, *Lipids*, 1973, **8**, 606.
34 M. H. C. Resurreccion-Magno, I. M. Villaseñor, N. Harada and K. Monde, *Phytother. Res.*, 2005, **19**, 246.
35 R. Srivastava, A. K. Shaw and D. K. Kulshreshtha, *Phytochemistry*, 1995, **38**, 687.
36 A. Zielińska, E. Kowalska, J. W. Sobczak, I. Łącka, M. Gazda, B. Ohtani, J. Hupka and A. Zaleska, *Sep. Purif. Technol.*, 2010, **72**, 309.
37 S. Biniak, G. Szymański, J. Siedlewski and A. Światkowski, *Carbon*, 1997, **35**, 1799.
38 S. Saha, J. Wang and A. Pal, *Sep. Purif. Technol.*, 2012, **89**, 147.
39 J. Jiménez, H. Liu and E. Fachini, *Mater. Lett.*, 2010, **64**, 2046.
40 G. Wertheim, S. DiCenzo and D. Buchanan, *Phys. Rev. B*, 1986, **33**, 5384.
41 S. Shanmugam, B. Viswanathan and T. K. Varadarajan, *Nanoscale Res. Lett.*, 2007, **2**, 175.
42 H. S. Shin, H. C. Choi, Y. Jung, S. B. Kim, H. J. Song and H. J. Shin, *Chem. Phys. Lett.*, 2004, **383**, 418.
43 K. T. V. Rao, P. S. S. Prasad and N. Lingaiah, *Green Chem.*, 2012, **14**, 3436.
44 S. D. Standridge, G. C. Schatz and J. T. Hupp, *Langmuir*, 2009, **25**, 2596.
45 N. C. Jeong, C. Prasittichai and J. T. Hupp, *Langmuir*, 2011, **27**, 14609.
46 A. Listorti, C. Creager, P. Sommeling, J. Kroon, E. Palomares, A. Fornelli, B. Breen, P. R. F. Barnes, J. R. Durrant and C. Law, *Energy Environ. Sci.*, 2011, **4**, 3494.
47 Q. Wang, J. E. Moser and M. Grätzel, *J. Phys. Chem. B*, 2005, **109**, 14945.
48 K. S. Kim, H. Song, S. H. Nam, S. M. Kim, H. Jeong, W. B. Kim and G. Y. Jung, *Adv. Mater.*, 2012, **24**, 792.
49 Y. S. Chen, C. Li, Z. H. Zeng, W. B. Wang, X. S. Wang and B. W. Zhang, *J. Mater. Chem.*, 2005, **15**, 1654.
50 M. Planells, L. Pellejà, J. N. Clifford, M. Pastore, F. De Angelis, N. López, S. R. Marder and E. Palomares, *Energy Environ. Sci.*, 2011, **4**, 1820.

